

Modeling of a Fluidized Bed Membrane Reactor for the Steam Reforming of Methane: Advantages of Oxygen Addition for Favorable Hydrogen Production

M. A. Rakib and K. I. Alhumaizi*

Department of Chemical Engineering, College of Engineering, King Saud University, Riyadh, Saudi Arabia

Received April 4, 2005. Revised Manuscript Received July 5, 2005

A bubbling fluidized bed membrane reactor for steam reforming of methane is mathematically investigated, with the permselective Pd membranes removing hydrogen from the reaction system to enhance the methane conversion. Oxygen fed into the reaction system can decrease the endothermicity of the overall reaction by the combustion of methane, thereby reducing the need of external firing. Operation at low feed steam–carbon ratios is also possible with the steam required for the reforming reaction being provided as a product from the combustion reactions, although problems related to coking also need to be addressed at very low ones. A drop in the reactor temperature at the inlet of the reactor itself due to the high endothermicity and fast kinetics of the steam reforming reactions does not strongly support the idea of a higher feed temperature favoring the reaction conversion. Thereafter, in situ generation of heat by the combustion reactions is a more effective means to give better reactor performance, and a higher feed temperature can be used to supplement this performance. However, since higher oxygen–methane ratios also tend to consume more of the methane itself, this cannot be increased much and an optimum value exists with respect to the favorable production of pure hydrogen from the reactor permeate side.

Introduction

Hydrogen is fast emerging as a clean energy source as an alternative to the existing fossil fuels, and truly, it is being framed as the energy currency of the future.¹ In addition, the demand of pure hydrogen is ever increasing in the petrochemical industries as a feedstock for a wide range of products and also in the petroleum processing industries for preliminary hydroprocessing of a wide range of feedstock. Hydrocracking and hydrodesulfurization rank second in hydrogen consumption, only behind ammonia synthesis, which is the largest user of steam reforming. Clean energy applications such as fuel cells and rocket fuels are also other important aspects of hydrogen usage. Also of high importance is the application of synthesis gas for a variety of processes such as production of methanol, Fischer–Tropsch synthesis, oxo-synthesis, and as a reduction gas for the direct reduction of iron.

Hydrogen from methane has gained a position of high importance in the present industrial scenario, courtesy of the availability of great reserves of natural gas worldwide. Deteriorating quality of petroleum crude, progressively stringent petroleum products specifications, and tougher environmental regulations have further focused world attention toward this source for the generation of hydrogen and synthesis gas needed in the industry.

The traditional fixed-bed steam reformer for methane has obvious limitations of its own. Diffusional limitations result to very low effectiveness factors of the order of 10^{-2} to 10^{-3} .^{2,3} Also formation of hot spots leads to problems related to precise temperature control. Pressure drop limitations again bar any attempt to improve the effectiveness factor by using smaller diameter particles. Adris⁴ came up with a novel idea of a fluidized bed steam reformer, with the heat being supplied through immersed heat transfer tubes.

The phenomenon of selective permeation of hydrogen through Pd membrane has also been utilized by researchers^{5,6} to break the thermodynamic equilibrium limitations of the MSR reaction and, hence, improve the reaction conversion. The concept of a Pd membrane reactor is also very relevant for the production of ultrapure hydrogen, avoiding catalyst poisoning by CO.

(1) Adris, A. M. A fluidized bed membrane reactor for steam methane reforming: experimental verification and model validation. Ph.D. Thesis, University of British Columbia, Vancouver, Canada 1994.

(2) De Deken, J. C.; Devos, E. F.; Froment, G. F. Steam reforming of natural gas. *Chemical Reaction Engineering ACS Symposium Series*; American Chemical Society: Washington, DC, 1982; p 196.

(3) Soliman, M. A.; Elnashaie, S. S. E. H.; Al-Ubaid, A. S.; Adris, A. M. Simulation of steam reforming for methane. *Chem. Eng. Sci.* **1988**, *43* (8), 1801–1806.

(4) Adris, A. M. A fluidized bed steam reformer for methane reforming. M.Sc. Thesis, University of Salford, Salford, England, 1989.

(5) Adris, A.; Elnashaie, S. S. E. H.; Hughes, R. Fluidized bed membrane steam reforming of methane. *Can. J. Chem. Eng.* **1991**, *69*, 1061–1070.

(6) Adris, A. M.; Lim, C. J.; Grace, J. R. The fluidized bed membrane reactor for steam methane reforming: model verification and parametric study. *Chem. Eng. Sci.* **1997**, *52*, 1609–1622.

* Corresponding author: Tel: +966-14676813. Fax: +966-14678770. E-mail: humaizi@ksu.edu.sa.

Widely accepted and used reaction kinetics for this process is the reaction scheme by Xu and Froment.⁷ The earlier kinetics^{2,8} have been shown to be limited in their range of applicability and capability to demonstrate behavior of reaction rates with varying steam partial pressures.⁹ The kinetic expressions by Xu and Froment⁷ was analyzed, and a non-monotonic dependence of the reaction rate upon the steam partial pressure was predicted. This indicates the existence of an optimum partial pressure of steam in the feed gas mixture to maximize the conversion of methane. As an extension to this deduction, for a given set of operating conditions, there is supposed to be an optimum steam–methane ratio for the maximization of hydrogen production. The carbon deposition over the catalyst in a Pd–Ag membrane reactor for the MSR reaction has been analyzed.¹⁰ In membrane reactors, a higher steam–methane ratio than those in traditional reactors had to be used to avoid carbon formation due to hydrogen removal from the reaction volume. This fact has also to be maintained while optimizing this ratio for maximizing hydrogen production.

Controlled oxygen input with the feed has been proposed to provide the heat requirement of the otherwise endothermic reaction system, creating an autothermal reaction system.¹¹ The mixing of solids in the fluidized bed suppresses catalytic deactivation in the MSR reaction since carbon deposits can be burnt out in the oxygen-rich distributor. This series of concepts led to intensive research for a fluidized bed membrane reactor for the steam reforming of methane with the addition of oxygen with feed.

As has been observed, higher temperature increases the conversion of the reaction. However, the overall behavior of the steam reforming reaction for methane is highly endothermic, and the high reaction rate results in a rapid decline in the reactor temperature. This warrants external firing, as in conventional reformers, to maintain a fairly reasonable reactor temperature for higher hydrogen output. It has been shown that the addition of oxygen along with the feed can decrease the endothermicity of the reaction. Steam reforming coupled with this process of partial combustion of methane, termed as an autothermal reforming process, can maintain a reasonable reforming temperature without substantial or zero external firing.¹¹ In addition, oxygen addition has the advantage of decreasing the amount of carbon deposited on the catalyst, attributable to the ensemble size control by oxygen, which covers a fraction of the nickel surface, decreasing the particle size, and inhibiting the polymerization of carbon and, consequently, its accumulation.¹² On the other hand, with simultaneous oxygen feed to the reactor for maintaining

the reactor autothermal behavior the feed methane is consumed resulting in a drop of the hydrogen yield. So, again there has to be an optimum oxygen–methane ratio to maximize hydrogen production so that the advantages of oxygen addition offset the sacrificial consumption of methane.

Equilibrium modeling of the steam methane reforming process with oxygen addition has been studied, and it has been shown that methane conversions increase with an increase in temperature, oxygen-to-methane feed ratio, and steam-to-methane ratio.¹³ These results also show that hydrogen permeation as well as oxygen addition may decrease the probability of coke formation on the catalyst and the permeable membrane tubes. Fluidized bed membrane reactors with oxygen, with and without immersed permeable tubes, have been simulated and have demonstrated the advantages of oxygen addition.¹⁴ “Hydrogen yields are lower for autothermal operation, but the penalty is likely to be worthwhile except in very small units given the disadvantages in current industrial steam reformers”. A methodology to deduce an optimization strategy for maximizing the hydrogen yield with respect to $O_2/(CH_4 \text{ feed})$ has been shown.¹⁵ They recommend operation at the highest possible SCR and inlet feed temperature, while minimizing heat loss and reactor pressure.

Novel reactor configurations have been proposed, the third generation reformer, with a circulating fluidized bed reactor with membrane separation of hydrogen and oxygen input using membranes to separate it from air.^{16,17} It has been also shown that autothermal operations give high hydrogen yields and productivities with net low consumption of energy. A similar configuration was studied¹⁸ and shown how a combination of the endothermic steam reforming and exothermic oxidative reforming of methane gives this circulating fast fluidized bed membrane reformer (CFFBMR) advantages of producing hydrogen with high yields and energy saving benefits. Parametric studies and optimization for this setup have shown that this can lead to an efficient production of hydrogen at relatively low temperatures, high pressures, and low steam-to-carbon ratios.¹⁹ This configuration can be physically realized with experimental studies being conducted by Ritchie et al.,²⁰ which

(7) Xu, J.; Froment, G. F. Methane steam reforming, methanation, and water-gas shift: I. Intrinsic kinetics. *AIChE J.* **1989**, *35* (1), 88.

(8) Bodrov, N. M.; Apel'baum, L. O.; Temkin, M. I. Kinetics of the reactions of methane with steam on the surface of nickel. *Kinet. Katal.* **1964**, *5*, 696–705.

(9) Elnashaie, S. S. E. H.; Adris, A. M.; Al-Ubaid, A. S.; Soliman, M. A. On the non-monotonic behavior of methane-steam reforming kinetics. *Chem. Eng. Sci.* **1990**, *45* (2), 491.

(10) Jorgensen, S. L.; Nielsen, P. E. H.; Lehrmann, P. Steam reforming of methane in a membrane reactor. *Catal. Today* **1995**, *25*, 303–307.

(11) Roy, S.; Pruden, B. B.; Adris, A. M.; Lim, C. J.; Grace, J. R. Fluidized-bed steam methane reforming with oxygen input. *Chem. Eng. Sci.* **1999**, *54*, 2095–2102.

(12) Dias, J. A. C.; Assaf, J. M. The advantages of air addition on the methane steam reforming over Ni/ γ -Al₂O₃. *J. Power Sources* **2004**, *137* (2), 264–268.

(13) Grace, J. R.; Li, X.; Lim, C. J. Equilibrium modeling of catalytic steam reforming of methane in membrane reactors with oxygen addition. *Catal. Today* **2001**, *64*, 141–149.

(14) Dogan, M.; Posarak, D.; Grace, J.; Adris, A. M.; Lim, C. J. Modeling of autothermal steam methane reforming in a fluidized bed membrane reactor. *Int. J. Chem. Reactor Eng.* **2003**, *1*, Article A2.

(15) Hagh, B. F. Optimization of autothermal reactor for maximum hydrogen production. *Int. J. Hydrogen Energy* **2003**, *28* (12), 1369–1377.

(16) Prasad, P.; Elnashaie, S. S. E. H. Novel circulating fluidized bed membrane reformer for the efficient production of ultraclean fuels from hydrocarbons. *Ind. Eng. Chem. Res.* **2002**, *41* (25), 6518.

(17) Prasad, P.; Elnashaie, S. S. E. H. Coupled steam and oxidative reforming for hydrogen production in a novel membrane circulating fluidized bed reformer. *Ind. Eng. Chem. Res.* **2003**, *42* (20), 4715–4722.

(18) Chen, Z.; Yan, Y.; Elnashaie, S. Novel circulating fast fluidized-bed membrane reformer for efficient production of hydrogen from steam reforming of methane. *Chem. Eng. Sci.* **2003**, *58*, 4335–4349.

(19) Chen, Z.; Prasad, P.; Yan, Y.; Elnashaie, Y. Simulation of steam reforming of natural gas with oxygen input in a novel membrane reformer. *Fuel Process. Technol.* **2003**, *83*, 235–252.

(20) Ritchie, J. T.; Richardson, J. T.; Luss, D. Ceramic membrane reactor for synthesis gas production. *AIChE J.* **2001**, *47* (9), 2092–2101.

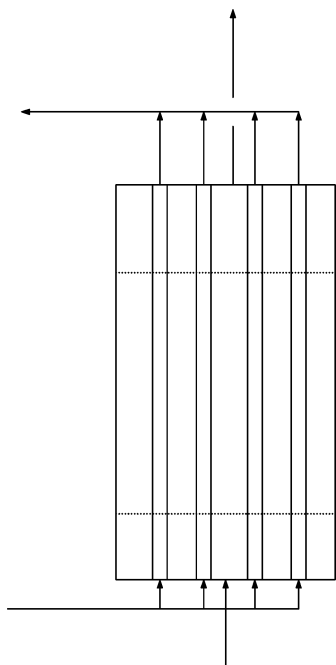


Figure 1. Schematic diagram of the reactor.

suggest that it should be possible to develop a commercial process for production of syngas using ceramic membranes while avoiding the need for separation of the nitrogen either before or after the reaction.

This work deals with parametric studies of performance of a fluidized bed MSR reactor with oxygen input, and establishing the oxygen–methane ratio and the steam–methane ratio as important parameters for performance optimization of the steam reformer, and for emphasizing that oxygen addition rather than high feed temperatures is a better option for maximizing hydrogen permeate yields.

Higher reactor pressure leads to a lower methane conversion, as is evident from the thermodynamic behavior, and also due to the consequent increase in the gas velocity. However, higher hydrogen partial pressure differential between the reactor side and the sweep gas enhances hydrogen permeation toward the sweep side and, hence, increases methane conversion beyond equilibrium. In this case again, depending on the permeation capacity (which again is a function of the membrane thickness), there might be some optimum reactor pressure to maximize CH_4 conversion and hydrogen yield. However, for the present studies, a reactor pressure of 26 bar, on the lines of the paper⁶ is maintained for the simulation runs. The mechanical stability of the Pd membranes for such operating conditions need to be further investigated experimentally.

Mathematical Model

Reactor Configuration. The schematic diagram of the reactor as considered for the modeling is shown in Figure 1.

Zone 1 is the bubbling fluidized bed at the entrance region. It is modeled as two phases (viz., the bubble and dense phase) in plug flow with species exchange among themselves. Due to the mechanical constraints, the membrane tubes in this zone do not allow hydrogen permeation. Zone 2 is modeled similar to the zone 1,

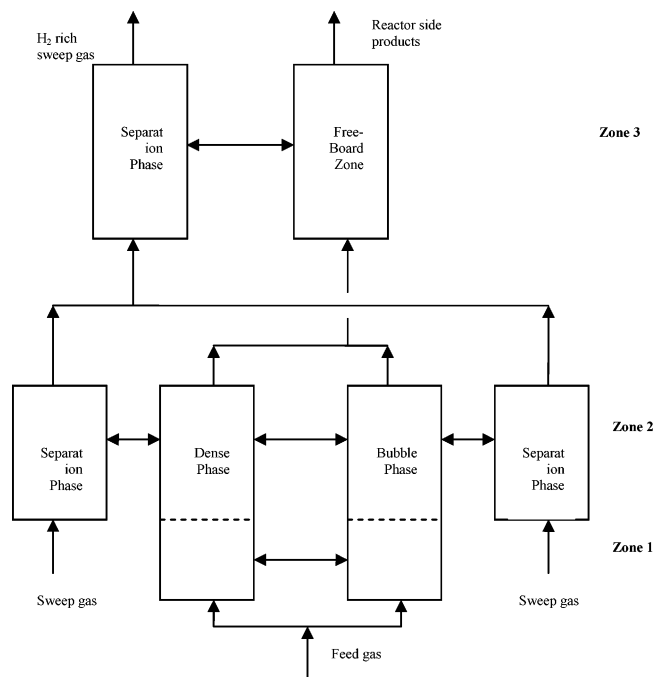


Figure 2. Schematic diagram of the events considered in modeling.

but here the permselective membrane tubes allow preferential hydrogen separation from the reaction zone to the sweep gas side. Zone 3 is the single-phase dilute phase, with reactions continuing to occur on the entrained solid catalyst particles, assisted by membrane separation of hydrogen. The events in these three zones are outlined in Figure 2.

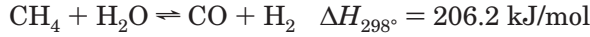
Assumptions. The current model is developed on the lines of Adris et al.⁶ with the following assumptions:

- (1) Steady-state reactor conditions.
- (2) The reactor is modeled as two regimes: the lower dense catalyst bed and the lean freeboard regime with low solid holdup. The lower dense catalyst bed is treated as two parallel phases made up of the dense phase and a bubble phase. The freeboard regime is treated as a single phase plug flow.
- (3) Most of the reactions take place in the dense phase in the lower regime, and plug flow behavior is assumed. Reactions occur to a lesser extent on the low concentration of catalyst particles in the bubble phase also, and plug flow behavior is assumed.
- (4) The freeboard region also undergoes chemical reaction over the surface of entrained catalyst particles. Solids loading in dilute phase has been taken to decay exponentially with height.
- (5) Catalyst diffusion resistance is taken to be negligible.
- (6) Sweep and permeating gases are also assumed to be in plug flow.

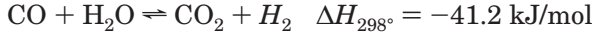
Rate Expressions. The rates of chemical reactions were calculated using the following kinetic model using the $\text{Ni}/\alpha\text{-Al}_2\text{O}_3$ catalyst.²¹

For the steam reforming reactions:

(21) De Groot, A. M.; Froment, G. F. Simulation of the catalytic partial oxidation of methane to synthesis gas. *Appl. Catal. A* **1998**, *138*, 127–133.



$$r_1 = k_1 \left(\frac{P_{\text{CH}_4} P_{\text{H}_2\text{O}}}{P_{\text{H}_2}^{2.5}} - \frac{P_{\text{CO}} P_{\text{H}_2}^{0.5}}{K_1} \right) / \text{DEN}^2 \quad (1)$$



$$r_2 = k_2 \left(\frac{P_{\text{CO}} P_{\text{H}_2\text{O}}}{P_{\text{H}_2}} - \frac{P_{\text{CO}_2}}{K_2} \right) / \text{DEN}^2 \quad (2)$$

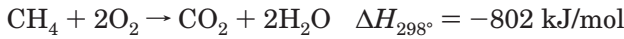


$$r_3 = k_3 \left(\frac{P_{\text{CH}_4} P_{\text{H}_2\text{O}}^2}{P_{\text{H}_2}^{3.5}} - \frac{P_{\text{CO}_2} P_{\text{H}_2}^{0.5}}{K_1 K_2} \right) / \text{DEN}^2 \quad (3)$$

where

$$\text{DEN} = 1 + K_{\text{CO}} P_{\text{CO}} + K_{\text{H}_2} P_{\text{H}_2} + K_{\text{CH}_4} P_{\text{CH}_4} + \frac{K_{\text{H}_2\text{O}} P_{\text{H}_2\text{O}}}{P_{\text{H}_2}} \quad (4)$$

For the combustion of methane:



$$r_4 = \frac{k_4 x_{\text{CH}_4} x_{\text{O}_2}}{(1 + KE_4 x_{\text{CH}_4} + KE_5 x_{\text{O}_2})} + \frac{k_5 x_{\text{CH}_4} x_{\text{O}_2}^{0.5}}{(1 + KE_4 x_{\text{CH}_4} + KE_5 x_{\text{O}_2})^2} \quad (5)$$

where x_{CH_4} and x_{O_2} are mole fractions of methane and oxygen, respectively, as percentages. The kinetic rate coefficients and adsorption equilibrium coefficients are tabulated in Appendix A.

Hydrogen Flux through the Pd Membranes. The permeation flux of hydrogen through the Pd membranes is taken to be calculated as:

$$J_{\text{H}_2} = P_{\text{M}} \frac{P_{\text{H}_2,\text{R}}^{0.5} - P_{\text{H}_2,\text{S}}^{0.5}}{\delta} \quad (6)$$

$$P_{\text{M}} = P_{\text{M}0} \exp\left(\frac{-E_{\text{P}}}{RT}\right) \quad (7)$$

The values of the permeation parameters are taken from Adris¹ as:

$$P_{\text{M}0} = 3.21 \times 10^{-7} \text{ mol}/(\text{m}\cdot\text{s}\cdot\text{Pa}^{0.5})$$

[preexponential factor for permeation]

$$E_{\text{P}} = 20.5 \text{ kJ/mol}$$

[activation energy for permeation]

Surface area used to calculate the H_2 molar flow is $\pi d_i L$. $P_{\text{H}_2,\text{R}}$ and $P_{\text{H}_2,\text{S}}$ are the hydrogen partial pressures in the reactor side and the sweep gas side, respectively.

Fluidized Bed Hydrodynamics. The hydrodynamic relationships for the fluidized bed reactor are given in Appendix B

Model Equations for Reactor Side. There are six components (CH_4 , H_2O , CO , CO_2 , H_2 , and O_2) involved in the four reactions considered above.

Mole Balance for i th Species for the Bubble Phase.

$$\frac{dF_i^{\text{b}}}{dL} = K'_i \alpha^{\text{b}} \epsilon^{\text{b}} A (C_i^{\text{d}} - C_i^{\text{b}}) + \Phi^{\text{b}} \rho_{\text{p}} A \sum_{j=1}^4 \gamma_{ij} R_j^{\text{b}} - \epsilon^{\text{b}} Q_i^{\text{b}} \quad i = 1, 2, \dots, 6 \quad (8)$$

Mole Balance for i th Species for the Dense Phase.

$$\frac{dF_i^{\text{d}}}{dL} = K'_i \alpha^{\text{d}} \epsilon^{\text{d}} A (C_i^{\text{b}} - C_i^{\text{d}}) + \Phi^{\text{d}} \rho_{\text{p}} A \sum_{j=1}^4 \gamma_{ij} R_j^{\text{d}} - \epsilon^{\text{d}} Q_i^{\text{d}} \quad i = 1, 2, \dots, 6 \quad (9)$$

where the superscripts b and d refer to the bubble and dense phases, respectively; γ_{ij} is the stoichiometric coefficient of component i in the j th reaction (negative for species consumed and positive for the products); and Q_i^{b} and Q_i^{d} are the permeation rates per unit length from the reactor side to the sweep gas side for the bubble phase and the dense phases, respectively, for species i . The permeation rate per unit length for hydrogen is calculated from the permeation flux through Pd membrane as described before and is zero for all other species.

For zone 1, the permeation rate is taken to be zero, keeping in view the mechanical aspects of the membrane fittings. For zone 2, both the bubble and dense phase reactions assisted with membrane separation for hydrogen are considered. For zone 3, reactions occur in the single dilute phase considered, assisted by membrane separation.

Model Equations for Separation Side. The differential mole balance equation for the permeate hydrogen in the two-phase zone (zone 2) is

$$\frac{dF_{\text{H}_2}^{\text{S}}}{dL} = \epsilon^{\text{b}} Q_{\text{H}_2}^{\text{b}} + \epsilon^{\text{d}} Q_{\text{H}_2}^{\text{d}} \quad (10)$$

and in the single dilute phase zone 3 is

$$\frac{dF_{\text{H}_2}^{\text{S}}}{dL} = Q_{\text{H}_2}^{\text{dil}} \quad (11)$$

For zone 1,

$$\frac{dF_{\text{H}_2}^{\text{S}}}{dL} = 0 \quad (12)$$

Model Equations for Energy Balance. The differential energy balance equation can be expressed as

$$\frac{dT}{dL} = \frac{\dot{Q} - A \rho_{\text{p}} \sum_{j=1}^4 R_j \Delta H_{\text{r}j}}{\sum_{i=1}^6 n_i \left(C_{pi} + T \frac{dC_{pi}}{dT} \right)} \quad (13)$$

where T is the reactor temperature, and \dot{Q} is the external heat input per unit bed height. For the non-isothermal modeling case, an adiabatic behavior is

Table 1. Reactor Dimensions and the Base Operating Conditions

reactor diameter	2.0 m	reactor pressure	2.6 MPa
expanded bed height	12.0 m	permeate side pressure	0.2 MPa
freeboard height	4.0 m	CO feed rate	1×10^{-8} kmol/h
distributor hole diameter	1 mm	CO ₂ feed rate	1×10^{-8} kmol/h
distributor number of holes	16478	H ₂ feed rate	0.25 kmol/h
catalyst solid density	3350 kg/m ³	sweep gas flow rate	175 kmol/h
mean particle size	174 μm	CH ₄ feed rate	175 kmol/h
number of membrane tubes	2848		
inner diameter of Pd tube	4.22 mm		
outer diameter of Pd tube	4.70 mm		

assumed, with $\dot{Q} = 0$. For the isothermal case, $dT/dL = 0$.

Interphase Mass Exchange Coefficient. The interphase mass exchange coefficient for the modeling purpose is calculated using the correlation.²² For the i th component:

$$K_i' = \frac{U_{mf}}{3} + \left(\frac{4D_{ie}\epsilon_{mf}U_b}{\pi d_b} \right)^{1/2} \quad (14)$$

D_{ie} is the effective diffusivity of the component i in the gas mixture and is calculated based on the average composition of the bubble and the dense phases, using the following:²³

$$\frac{(1 - x_i)}{D_{ie}} = \sum_{i=1}^n \left(\frac{x_i}{D_{ij}} \right) \quad (15)$$

where D_{ij} is the binary diffusivity of components i and j , provided i is not equal to j .

Data for the FBMR. The reactor dimensions and the base operating conditions which were held constant are given in Table 1.¹⁴ A small feed rate of 0.25 kmol/h for H₂ is adopted for the simulations so that the rate expressions for the reforming reactions do not give infinite values. Similarly, a nominal value of 1×10^{-8} kmol/h has been adopted for the CO and CO₂ feed rates to avoid numerical instabilities in the simulations. In the simulations, lengths of the three zones are 0.5, 11.5, and 4.0 m, respectively.

Case 1: Isothermal Studies for O₂ Flow Rate and Steam–Carbon Ratio. Isothermal studies were carried out for four different temperatures, incorporating oxygen injection. It should be borne in mind that although the principal idea behind oxygen injection is to maintain a reasonable reaction temperature, this study is done for comparison purposes with the non-isothermal cases under similar conditions. Four temperatures (viz., 500, 750, 850, and 1000 °C) were studied. Results of simulation are depicted in the form of three-dimensional plots.

Plots have been included for varying OMR and SCR. For this study, the ranges considered both for SCR and OMR are from 0 to 8. Figure 3 shows that for each temperature studied for the isothermal model, initially a higher SCR leads to higher production of total H₂, but this trend levels off at high SCRs. Total H₂ refers to the sum of the hydrogen product from the reactor side and that permeating into the sweep gas.

In general, as is evident from Figure 4, the permeate hydrogen yield decreases with increasing OMR. This is attributed to the increasing methane consumption and hence the depletion of the feed itself for the steam reforming reaction.

Also, it is clearly shown that for any OMR, the permeate hydrogen passes through a maximum as the SCR is varied. For a fixed OMR, this trend passes through a maximum. In agreement with the previous discussion, the value of this maximum goes on increasing with decreasing OMRs, the highest one being for almost zero oxygen feed (OMR $\sim 10^{-5}$ for simulation purposes).

An interesting observation for the effect of the oxygen flow rate is that steam reforming is also possible for zero feed steam, from the plots in Figure 4. In this case, the steam required for the reforming reactions is provided as a product from the combustion of methane. Only at lower SCRs, the trend of the permeate hydrogen yield with increasing OMR passes through a maximum. It increases initially, because combustion provides steam, the reactant for the reforming reaction. However increasing the oxygen feed rate beyond certain level results in the combustion reaction out-performing the reforming reaction, resulting in a fall in hydrogen permeate yield. This trend does not hold true once we have enough steam present in the feed stream, and we see a monotonic decrease in permeate hydrogen yield with increasing OMR.

Isothermal plots at different temperatures in Figures 3–6 show that as the temperature is increased, the production of total H₂, permeate hydrogen, and methane conversion increase. These can be interpreted from the vertical color codes associated with each plot. This is because higher temperatures increase the rate of hydrogen permeation through the Pd membrane, and at the same time, a higher temperature is favorable for the endothermic steam reforming reactions.

Figure 5 shows the behavior of the permeate hydrogen, with respect to the reactor hydrogen, and the total hydrogen flow rates. The permeate hydrogen flow rate gradually surpasses the hydrogen flow rate inside the reactor as the SCR is decreased from high values. This might be attributed to the increase in hydrogen partial pressure inside the reactor with decreasing steam partial pressures and steam for reaction still available in situ by methane combustion. Also, as the temperature is increased, the permeate hydrogen surpasses the reactor hydrogen more drastically, and this can be attributed to increased permeation rates at higher temperatures.

Case 2: Non-Isothermal Studies for O₂ Flow Rate and SCR. Non-isothermal studies were carried out for different feed temperatures, incorporating oxygen injection. The main purpose of injecting oxygen with

(22) Sit, S. P.; Grace, J. R. Effect of bubble interaction on interphase mass transfer in gas-fluidized beds. *Chem. Eng. Sci.* **1981**, *36*, 327–335.

(23) Wilke, C. R.; Lee, C. Y. Estimation of diffusion coefficients for gases and vapors. *Ind. Eng. Chem.* **1955**, *47*, 1253.

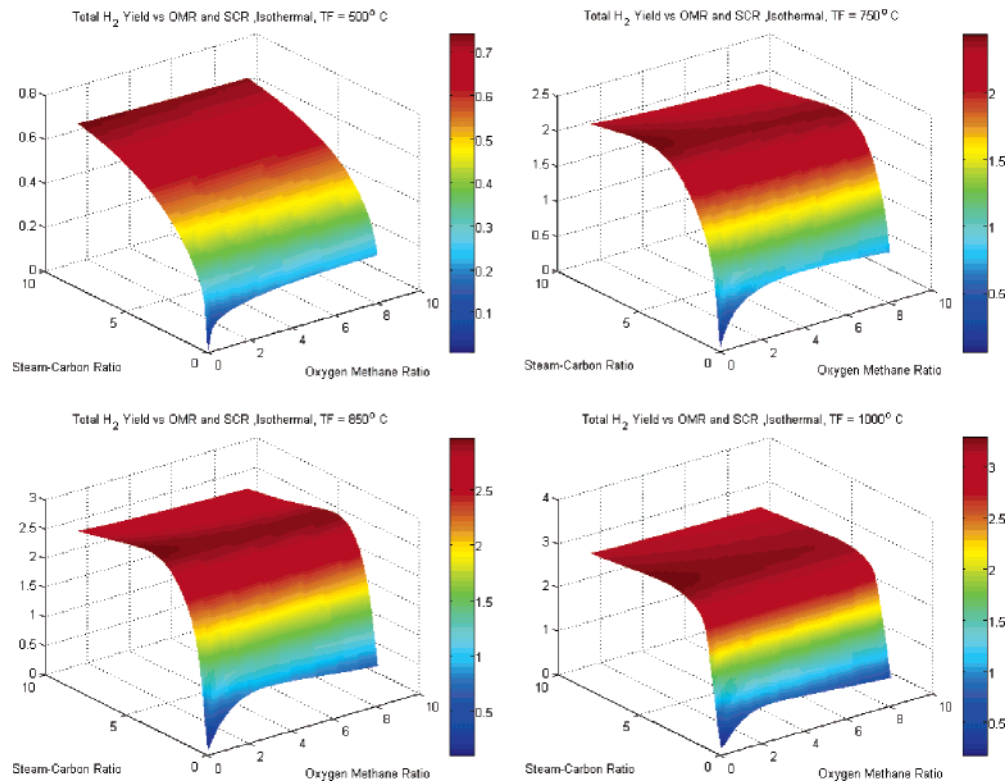


Figure 3. Total H₂ yield vs OMR and SCR, isothermal cases.

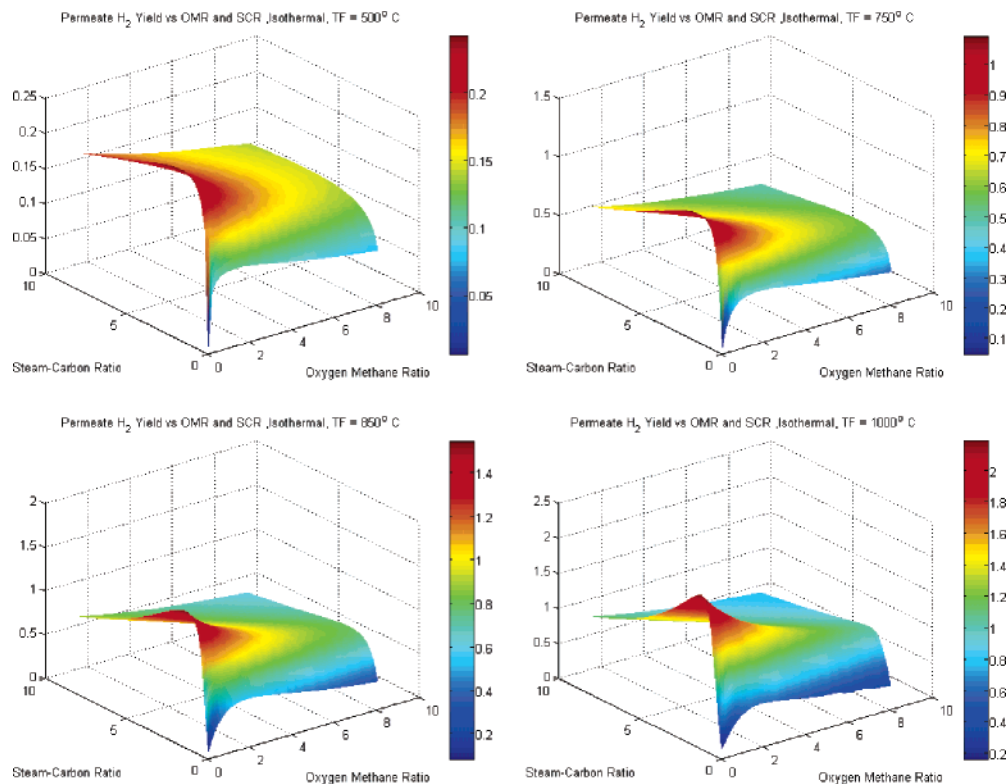


Figure 4. Permeate H₂ yield vs OMR and SCR, isothermal cases.

the feed is to supply the sensible heat in order to compensate for the endothermicity of the steam reforming reactions. Four feed temperatures (viz., 500, 750, 850, and 1000 °C) were studied. Results of simulation are depicted in the form of three-dimensional plots for varying OMR and SCR. For this study also, the ranges considered both for SCR and OMR are from 0 to 8.

Figures 7–9 show that when the steam reforming reaction and the combustion reaction of methane are considered in a non-isothermal model, the profiles of the hydrogen yields and the methane conversion are substantially affected by the increasing feed temperatures.

Figure 7 shows that for each temperature studied for the non-isothermal model, a higher SCR leads to higher

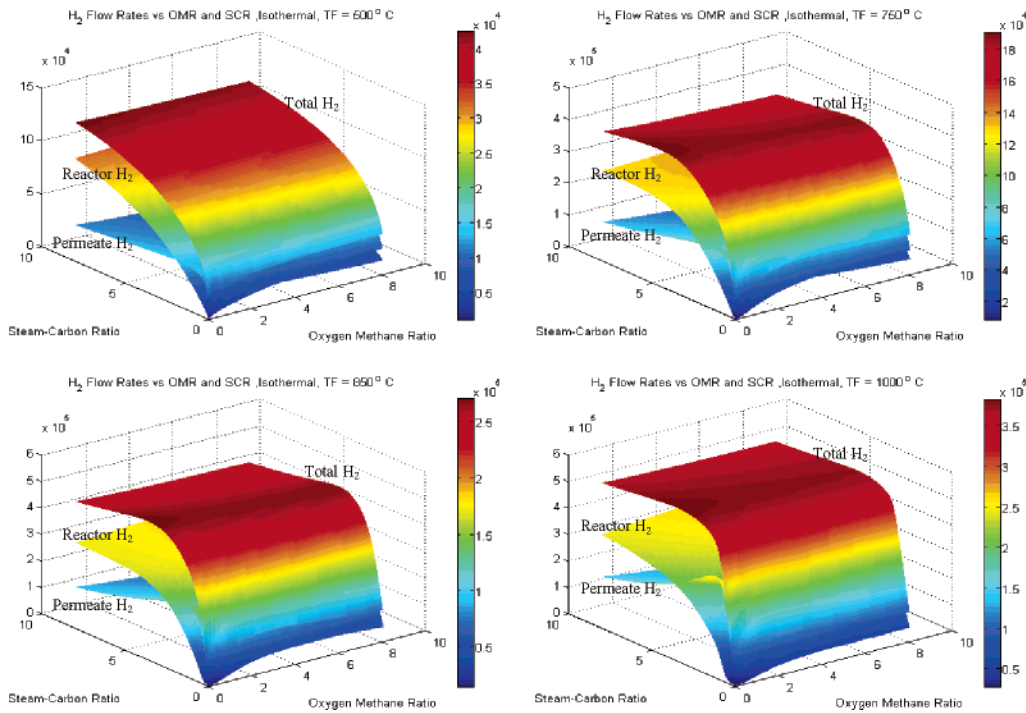


Figure 5. H₂ flow rates vs OMR and SCR, isothermal cases.

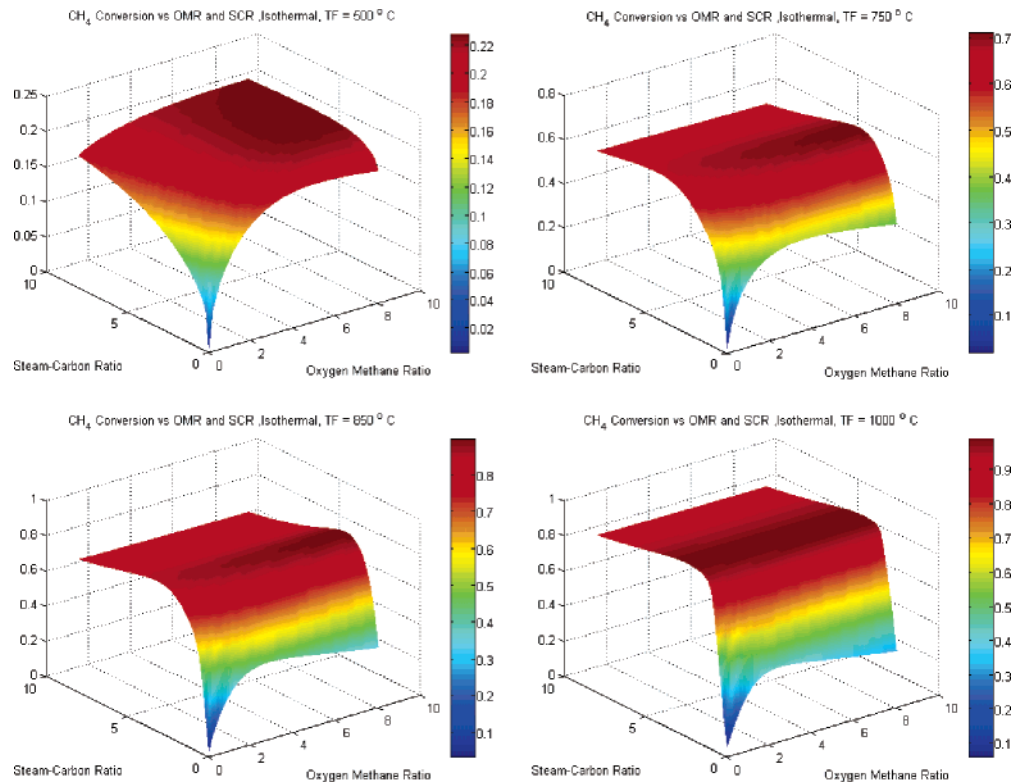


Figure 6. CH₄ conversions vs OMR and SCR, isothermal cases.

production of total H₂ at low OMR. For high OMRs, the total H₂ yield increases more drastically as the SCR is increased from zero but levels off soon at higher SCRs.

Effect of the oxygen feed rate is again a very interesting one in the non-isothermal case also. This effect is again more visible for lower SCRs. Only at lower SCRs, the trend of the total H₂ yield as well as the permeate H₂ yield with increasing OMR passes through a maximum. It increases initially, because combustion provides steam, the reactant for the reforming reaction. However,

the main intended role of introducing oxygen with the feed is to provide the sensible heat to compensate for the endothermicity of the steam reforming reactions, and the results are quite visible to meet the expectations.

The total H₂ yield in Figure 7 as well as the permeate hydrogen yield in Figure 8 passes through a maxima against the OMR at low SCRs. As in the isothermal case, this also can be explained out of two competitive phenomena. At low SCRs, as the steam partial pressure

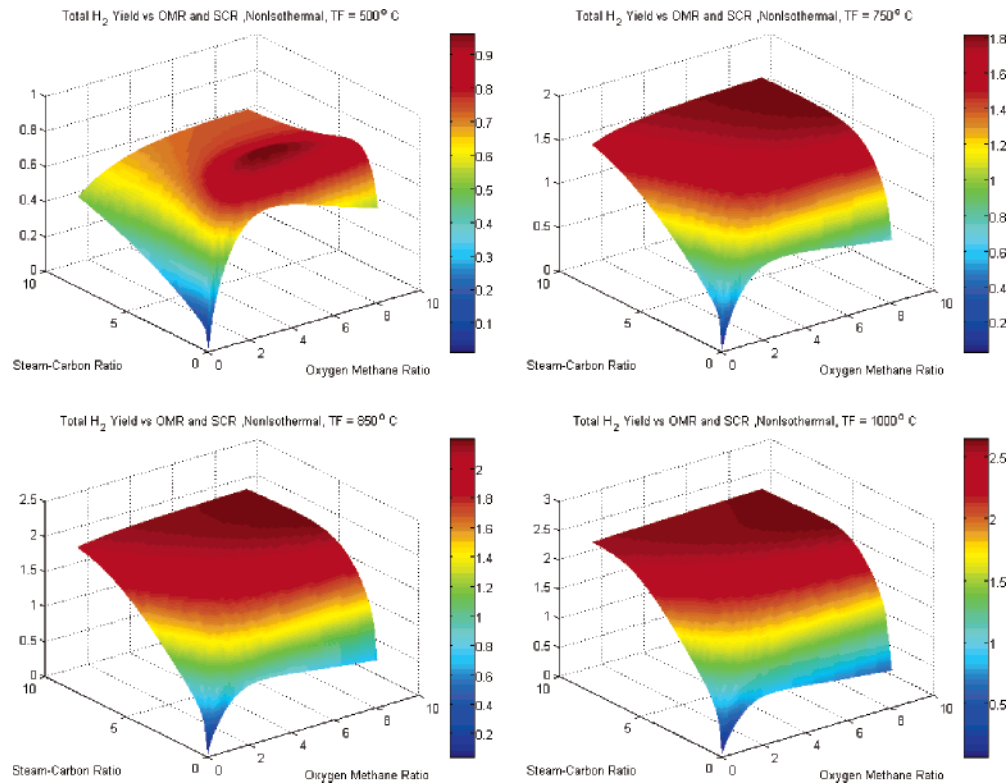


Figure 7. Total H_2 yield vs OMR and SCR, non-isothermal cases.

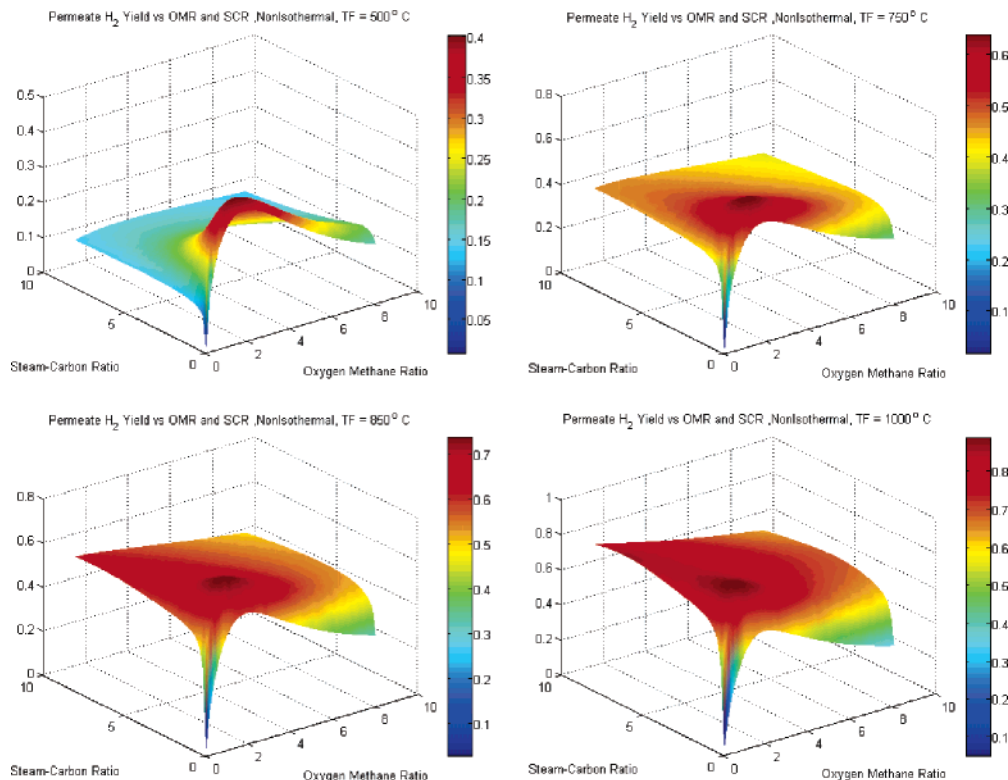


Figure 8. Permeate H_2 yield vs OMR and SCR, non-isothermal cases.

tends toward zero, the constraint comes from a very low partial pressure of one of the reactants; steam. However, at the same SCR, increasing the OMR results in a favorable forward reaction, generating hydrogen. A favorable partial pressure of steam for the reaction in this case come from the combustion of methane, which produces steam as well. However, increasing the OMR

beyond a certain limit consumes methane to unfavorable extents by combustion itself; hence, the hydrogen productions drop drastically. Unlike the isothermal case, this behavior with increasing oxygen feed rates still continues to exist for increasing SCRs in the feed, because in this case, the temperature “has” to be maintained by the combustion reaction, whereas in the

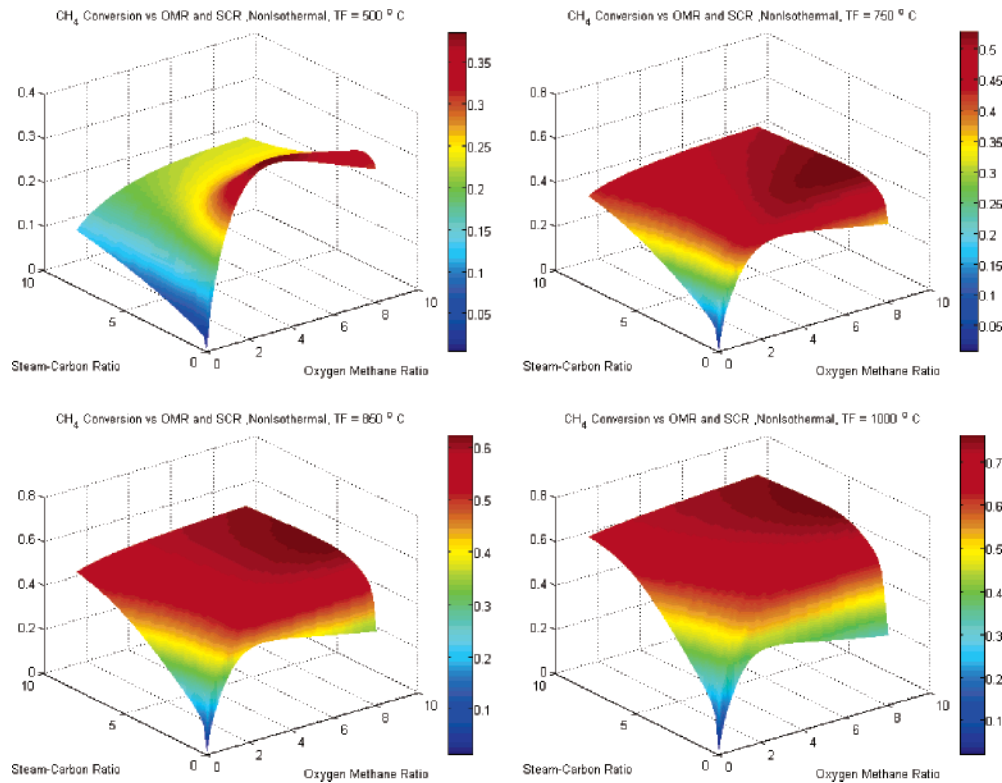


Figure 9. CH₄ conversions vs OMR and SCR, non-isothermal cases.

isothermal case, the temperature was maintained by external firing. For the non-isothermal case, at any SCR, irrespective of the feed temperature, the reactor temperature drops drastically; hence, the temperature increase out of combustion shows its effects.

These results indicate the possibility that addition of oxygen as a feed component in the reactor as a solution for the economic heat requirement for steam reforming of methane and that feasibility of operation in such a case at low steam feed rates might also be investigated. However, low SCR might lead to severe coke formation causing deactivation of the catalyst. Future solutions might necessitate the use of circulating fluidized bed membrane reactors instead of bubbling FBMRs, whereby a reactor–regenerator system can be introduced to re-activate the catalysts deactivated out of coke deposition at low steam flow rates.

Conclusions

A fluidized bed membrane reactor has been studied for the steam reforming of methane with immersed permeable Pd membrane tubes and addition of oxygen with the feed to generate the heat required to offset the endothermicity of the reaction. Effects of the OMR has been studied for both isothermal and non-isothermal behavior of the reactor. A drop in the reactor temperature at the inlet of the reactor itself due to the high endothermicity and fast kinetics of the steam reforming reactions does not make the idea of a higher feed temperature for favoring the reaction conversion attractive. Contrarily, in situ generation of heat by the combustion reactions, by introducing oxygen also with the feed is a more effective means to give better reactor performance. However, since higher OMRs also tend to consume more of the methane itself, this cannot be

increased much, and an optimum value exists with respect to the favorable production of pure hydrogen from the reactor permeate side. Also the hydrogen yields are lower when compared with cases for isothermal operations with external firing, but the overall ease of operation and possible lower costs than with the hassles and disadvantages of external firing can make it an attractive and feasible model. It has also been found that with oxygen injection with the feed, operation at low feed steam–carbon ratios, even tending toward zero, is possible with the steam required for the reforming reaction being provided as a product from the combustion reactions.

Having established steam reforming of methane being highly influenced by the injection of oxygen with the feed, it would be a fruitful exercise to explore the effects of different modes of this oxygen injection. If all the feed oxygen is introduced together with the natural gas and steam at the reactor feed, although the oxygen is supposed to be consumed only progressively and gradually along the reactor length, there would be an undesired sharing of the gas mixture enthalpy by bulk of entering oxygen as well as an undesired increase in reactor volume from the beginning itself. It is not desired to introduce the oxygen in bulk with the feed from the safety point of view as well and also because much of the methane might be lost through complete or severe oxidation. The alternative would be to inject optimum amount of O₂ along the reactor through the side at some fixed or variable intervals. The distribution of these injections can be optimized as per the amount of O₂ per injection, and so can be the number of and distance between the injections. Another viable alternative would be to introduce the oxygen through oxygen permselective membranes along the length of the re-

former. In addition, this permits air to be fed to reactor instead of pure oxygen and the possibility of producing pure nitrogen as an additional byproduct. Studies have been carried out.^{16,17,20} These objectives can be achieved effectively by optimizing the flow rate of air and controlling the thickness and permeability (material) of the oxygen permselective membranes.

Appendix A: Kinetics Rate Coefficients and Equilibrium Constants

Rate Coefficients.

$$k_1 \text{ (kmol bar}^{0.5} \text{ (kg of catalyst}^{-1} \text{ h}^{-1}) \text{)} = 4.225 \times 10^{15} \exp\left(-\frac{28879.0}{T}\right) \quad (\text{A.1})$$

$$k_2 \text{ (kmol bar}^{0.5} \text{ (kg of catalyst}^{-1} \text{ h}^{-1}) \text{)} = 1.955 \times 10^6 \exp\left(-\frac{8074.3}{T}\right) \quad (\text{A.2})$$

$$k_3 \text{ (kmol bar}^{0.5} \text{ (kg of catalyst}^{-1} \text{ h}^{-1}) \text{)} = 1.02 \times 10^{15} \exp\left(-\frac{29336.0}{T}\right) \quad (\text{A.3})$$

$$k_4 \text{ (kmol bar}^{-1} \text{ kg}^{-1} \text{ s}^{-1}) = 3.14 \times 10^{-7} \quad (\text{A.4})$$

$$k_5 \text{ (kmol bar}^{-1} \text{ kg}^{-1} \text{ s}^{-1}) = 2.64 \times 10^{-7} \quad (\text{A.5})$$

Adsorption Equilibrium Constants.

$$K_{\text{CO}} \text{ (bar}^{-1}) = 8.23 \times 10^{-5} \exp\left(-\frac{8497.71}{T}\right) \quad (\text{A.6})$$

$$K_{\text{CH}_4} \text{ (bar}^{-1}) = 6.65 \times 10^{-4} \exp\left(-\frac{4604.28}{T}\right) \quad (\text{A.7})$$

$$K_{\text{H}_2\text{O}} = 1.77 \times 10^5 \exp\left(-\frac{10666.35}{T}\right) \quad (\text{A.8})$$

$$K_{\text{H}_2} \text{ (bar}^{-1}) = 6.12 \times 10^{-9} \exp\left(-\frac{9971.13}{T}\right) \quad (\text{A.9})$$

$$\text{KE}_4 = 6.67 \times 10^{-2} \quad (\text{A.10})$$

$$\text{KE}_5 = 4.34 \times 10^{-5} \quad (\text{A.11})$$

Equilibrium Constants.

$$K_1 \text{ (bar}^2) = \exp\left(-\frac{26830}{T} + 30.114\right) \quad (\text{A.12})$$

$$K_2 = \exp\left(\frac{4400}{T} - 4.036\right) \quad (\text{A.13})$$

Appendix B: Hydrodynamic Relationships for the Fluidized Bed^{1,24}

The bubble size distribution is given by:

$$d_b = d_{\text{bm}} - (d_{\text{bm}} - d_{\text{b0}})e^{-0.3h/D} \quad (\text{B.1})$$

$$d_{\text{bm}} = 1.64[A(u_0 - u_{\text{mf}})]^{0.4} \quad (\text{B.2})$$

$$d_{\text{b0}} = \frac{1.38}{g^{0.2}} \left[\frac{A(u_0 - u_{\text{mf}})}{N_{\text{or}}} \right] \quad (\text{B.3})$$

The bubble rise velocity is given by:

$$u_b = u_0 - u_{\text{mf}} + 0.711(gd_b)^{1/2} \quad (\text{B.4})$$

The volume fraction of bed occupied by bubbles is given by:

$$\epsilon_b = \frac{(u_0 - u_{\text{mf}})}{u_b} \quad (\text{B.5})$$

The volume fraction of bed occupied by solids in dense phase is calculated as

$$\phi_d = (1 - \epsilon_b)(1 - \epsilon_{\text{mf}}) \quad (\text{B.6})$$

And the volume fraction of bed occupied by solids in bubble phase is calculated as $0.001\epsilon_b < \phi_b < 0.01\epsilon_b$. For this study, ϕ_b is taken to be $0.001\epsilon_b$.

The minimum fluidization velocity (u_{mf}) can be calculated from

$$A_r = \frac{\rho_g d_v^3 (\rho_p - \rho_g) g}{\mu^2} \quad (\text{B.7})$$

$$Re_{\text{mf}} = [(33.7)^2 + 0.0408A_r]^{1/2} - 33.7 \quad (\text{B.8})$$

The interphase mass transfer coefficient is then calculated as

$$k_{iq} = \frac{u_{\text{mf}}}{3} + \left[\frac{4D_{ie}\epsilon_{\text{mf}}u_b}{\pi d_b} \right] \quad (\text{B.9})$$

The gas distribution ratio between bubble and dense phase is given by:

$$R_{\text{db}} = \frac{u_0 - u_{\text{mf}}}{u_0} \quad (\text{B.10})$$

Nomenclature

A = cross-sectional area of bed, m²

C_i^b, C_i^d = concentration of species i in bubble and dense phases, respectively, mol/m³

$C_{p,i}$ = specific heat capacity of the species i , J/mol·K

d_b = bubble diameter, m

d_{bm} = maximum bubble diameter, m

d_{bo} = bubble diameter just above the distributor, m

d_p = mean particle diameter, m

D = reactor diameter

D_{ie} = effective molecular diffusivity of component i , m²/s

D_{ji} = binary diffusivity of components i and j , provided i is not equal to j

D_t = membrane tube diameter, m

E_P = activation energy for permeation

F_i = molar flow rate of species i in the feed, mol/s

F_i^b, F_i^d, F_i^s = molar flow rate of species j in bubble and dense phases and the sweep gas,

respectively, mol/s

F_T = total molar flow rate including all species along the bed cross-section

$-\Delta H_{vj}$ = heat of reaction j , J/mol

J_{H_2} = permeation flux of hydrogen through the Pd membranes, mol/m²·s

k_1, k_2, k_3 = rate constant for reactions 1–3, respectively, in steam reforming kinetics

K_4, k_5 = rate constants for reaction 4 in combustion kinetics

K_j = equilibrium constant for reaction j

$K_{CH_4}, K_{H_2}, K_{CO}, K_{H_2O}$ = adsorption constants for CH₄, H₂, CO, H₂O, respectively, in steam reforming kinetics

K'_i = interphase mass exchange coefficient for species i

KE_4, KE_5 = adsorption coefficients for CH₄ and O₂, respectively, in combustion kinetics

L = vertical distance measured from feed inlet

N = total number of membrane tubes

N_{or} = number of orifices in the distributor

OMR = oxygen to methane molar feed ratio

\dot{Q} = external heat input per unit bed height

$Q_{H_2}^b, Q_{H_2}^d, Q_{H_2}^{dil}$ = permeation rate of hydrogen per unit length from the bubble phase,

dense phase, and dilute phase, respectively, mol/m·s

P_i = partial pressure of species i , bars

$P_{H_2,R}$ = partial pressure of hydrogen in the reactor side, bar

$P_{H_2,S}$ = partial pressure of hydrogen in the sweep gas side, bar

P_{M0} = preexponential factor for permeation

R_i^b, R_i^d, R_i^{dil} = rate of reaction j in bubble phase, dense phase, and dilute phase,

respectively, mol/kg of catalyst·s

Re_{mf} = Reynolds number at minimum fluidization conditions

SCR = steam to carbon molar feed ratio

T = reactor temperature, K

u_b = velocity of a bubble rising through the bed, m/s

u_o = superficial gas velocity, m/s

u_{mf} = superficial gas velocity at minimum fluidization conditions, m/s

x_{CH_4}, x_{O_2} = mole fraction of methane and oxygen, respectively, as percentages

γ_{ij} = stoichiometric coefficient of species j in the i th reaction

δ = membrane thickness, m

ϵ_{mf} = bed voidage at minimum fluidization conditions

ϵ^b, ϵ^d = volume fraction of the catalyst bed occupied by the bubble and dense phase, respectively

μ = gas viscosity, kg/m·s

ρ_g = gas density, kg/m³

ρ_p = catalyst solid density, kg/m³

Φ^b, Φ^d = volume fraction of the catalyst bed occupied by solid particles in the bubble and dense phase, respectively

EF0500960